

Gravimetric Measurements and Theoretical Calculations of 4-Aminoantipyrine Derivatives as Corrosion Inhibitors for Mild Steel in Hydrochloric Acid Solution: Comparative Studies

Firas F. Sayyid¹, Ali M. Mustafa¹, Slafa I. Ibrahim², Mustafa K. Mohsin³,
Mahdi M. Hanoon¹, Mohammed H. H. Al-Kaabi⁴, A. A. H. Kadhum⁵,
Wan Nor Roslam Wan Isahak⁶, and A. A. Al-Amiery^{2,6,†}

¹Department of production Engineering and metallurgical, University of technology-Iraq, Baghdad 10001, Iraq

²Energy and Renewable Technology Centre, University of Technology, Baghdad, Iraq

³The Supreme National Authority for Accountability and Justice, Baghdad, Iraq

⁴Basrah University for oil and Gas, Basrah, Iraq

⁵Al-Ameed University, (A.H.K.) amir1719@gmail.com, Karbala, Iraq

⁶Department of Chemical and Process Engineering, Faculty of Engineering and Build Environment, Universiti Kebangsaan Malaysia, 43000 UKM Bangi, Selangor, Malaysia

(Received June 28, 2022; Revised July 02, 2022; Accepted July 03, 2022)

Due to continuous promotion of green alternatives to toxic petrochemicals by government policies, research efforts towards the development of green corrosion inhibitors have intensified recently. The objective of the current work was to develop novel green and sustainable corrosion inhibitors derived from 4-aminoantipyrine to effectively prevent corrosion of mild steel in corrosive environments. Gravimetric methods were used to investigate corrosion inhibition of 4-((furan-2-ylmethylene)amino)antipyrine (FAP) and 4-((pyridin-2-ylmethylene)amino)antipyrine (PAP) for mild steel in 1 M HCl. FAP and PAP were subjected to quantum chemical calculations using density functional theory (DFT). DFT was used to determine the mechanism of mild steel corrosion inhibition using inhibitors tested in HCl. Results demonstrated that these tested inhibitors could effectively inhibit mild steel corrosion in 1.0 M HCl. At 0.0005 M, these inhibitors' efficiencies for FAP and PAP were 93.3% and 96.5%, respectively. The Langmuir adsorption isotherm was obeyed by these inhibitors on the mild steel surface. Values of adsorption free energies, ΔG_{ads}^o , revealed that FAP followed chemical and physical adsorptions.

Keywords: 4-Aminoantipyrine, Furan, Pyridine, Corrosion inhibitor, Gravimetric

1. Introduction

Acid solutions, particularly hydrochloric acid, are well recognized to cause corrosion of alloys and metals if used for the removal of unwanted scale and rust in metal processing industries, oil-well acidizing in oil recovery, boiler cleaning, and other applications [1]. The use of HCl to increase the initial productivity of new wells or to recover the production of older wells leads to severe damage of the apparatus [2]. In these settings, industrial acid cleaners and acid purification treatments are exceedingly aggressive and can cause significant metal corrosion. Inhibitors are one of the numerous approaches to reduce metal corrosion, and they may be the safest and cheapest alternative [3–5]. Corrosion prevention of metallic structures has sparked a lot of interest because of the huge financial and

safety losses that corrosion has caused in numerous industries. Mild steel is an important construction material in a variety of industries since it is widely utilized and has a wide range of applications due to its low cost and excellent physical and mechanical characteristics [6]. Despite its widespread use, mild steel used in industry is susceptible to corrosion, particularly in acidic environments. As a result of its low corrosion protection, mild steel requires the development of specific corrosion protection technologies [7]. Corrosion is a prevalent issue with industrial metals, and it has a direct effect on their cost and safety. There are various techniques to prevent metal corrosion today, including optimizing metal components and smelting processes, organic/inorganic coating technologies, and the inclusion of corrosion inhibitors, the last of which is the most cost-effective and widely utilized [8–17]. At the right concentration, the inhibitors work by acting at the interface between the exposed metal surface and hostile media. In mineral acid solutions, compounds rich in heteroatoms such as nitrogen,

[†]Corresponding author: dr.ahmed1975@gmail.com,
dr.ahmed1975@ukm.edu.my

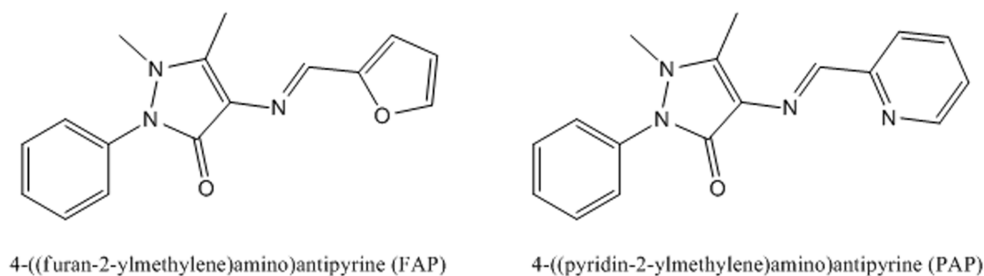


Fig. 1. Tested corrosion inhibitors

Table 4. Composition (wt %) of mild steel chemical samples

C	Mn	Si	Al	S	P	Fe
0.21%	0.05%	0.38%	0.01%	0.05%	0.09%	Balance%

oxygen, sulphur, and phosphorous, as well as multiple bonds found in aromatic rings or carbon chains, have been widely used as corrosion inhibitors [18–21]. The presence of a lone pair in heteroatoms and the planarity of molecules are also important aspects to consider when explaining the adsorption of inhibitor molecules onto metallic surfaces [22,23]. These inhibitors prevent degradation in two ways: I by forming a protective layer or an insoluble complex, and (ii) by their great propensity to adsorb on metallic surfaces. Aromaticity, electron density, functional groups and steric variables, as well as the type of the alloy and the corrosive environment, all have a part in corrosion inhibition action [24]. Corrosion molecules having heteroatoms such as phosphorus, sulphur, oxygen, and nitrogen atoms absorb rapidly on steel substrates, forming a layer of organic molecules-Fe complexes [25–31]. Purpose of providing efficient corrosion protection, the adsorbed layer works as a physical barrier between the metal substrate and the acidic solution [25–28]. These phenomena were used to prevent internal steel pipeline corrosion and unexpected dissolving of steel structures during the acidifying process; as a result, a corrosion inhibitor can increase the corrosion life of steel [30].

Two Schiff bases, 4-((furan-2-ylmethylene)amino)antipyrine and 4-((pyridin-2-ylmethylene)amino)antipyrine, were synthesized and tested as mild steel corrosion inhibitors in a 1 M HCl solution in this study. Temperature (303, 313, 323, and 333 K) influenced the corrosion inhibition efficacy of the synthesized Schiff bases.

In the study, gravimetric strategies were applied. In addition, quantum chemical computations and molecular simulations were used to determine the active centers that could be present. The molecular structures of the tested inhibitors are depicted in Fig. 1.

2. Materials and Methods

2.1 Corrosive Solution and Corrosion Inhibitors

Hydrochloric acid 37% (Merck-Malaysia) was diluted to 1 M with distilled water in the examined acidic environment. The

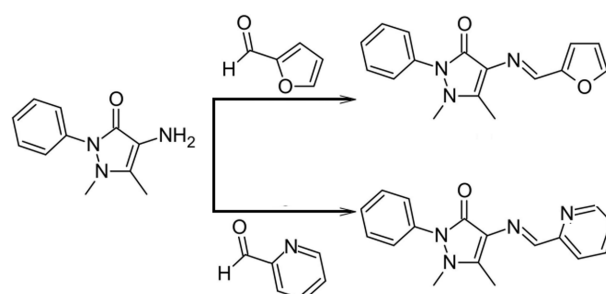


Fig. 14. The reaction synthesis of the tested inhibitors

concentration of examined inhibitors are currently in the kept ranging of 0.0001 to 0.0006 M.

2.2 Mild Steel

Elemental analysis of the mild steel alloy working electrode is displayed in Table 4 (weight %). The mild steel dimensions were $4.0 \times 2.5 \times 0.5 \text{ cm}^3$.

2.3 Synthesis of Corrosion Inhibitor

FAP and PAP were prepared according to literature procedure. See [31].

The chemical reaction of PAP synthesized is shown in Fig. 14.

2.4 Gravimetric Techniques

In these investigations, the usual exposure experimentation protocol outlined in TM0169/NACE/G31 [32] was followed. The gravimetric studies were carried out in a static environment. The examined media were kept at the desired temperature (303 K) in a water bath (programmable stirring hot plate). The mild steel coupons were suspended in the test solutions in triplicate for 1, 5, 10, 24, and 48 h. The concentrations of the examined inhibitors were 0.0001, 0.0002, 0.0003, 0.0004, 0.0005, and 0.0006 M. For all the experiments, the tested

corrosion inhibitor was dissolved firstly in ethyl alcohol (2 ml) and then added to acidic solution [33,34]. After the exposure times, the coupons were removed and treated to the ASTM standard G1-03 [35] post-treatment protocols. After 5 h of immersion, the effect of temperature (303, 313, 323, and 333 K), for various inhibitors concentrations was also studied. The tests were performed in triplicate and the average values were calculated.

Rate of corrosion (C_R) was determined based on weight loss as per the relation (21) [36]:

$$C_R = \frac{87600 \times W}{\rho at} \quad (21)$$

Where W represents the average weight loss in gram, ρ refers to the specimen density in $\text{g}\cdot\text{cm}^{-3}$, a is the specimen surface area in cm^2 and t is the exposure period in hours.

The inhibition efficiency was determined according to Equation (22):

$$IE\% = \frac{W_o - W_i}{W_o} \times 100 \quad (22)$$

Where W_o and W_i are the tested coupons weight losses in 1 M HCl environment in the absence and presence of tested inhibitors, respectively.

2.5 Quantum Calculation Method

Theoretical calculations were necessary to simulate the experimental data. Quantum chemical calculations were performed using density functional theory (DFT) to study the electronic structures of synthesized inhibitors to evaluate their theoretical properties. The current computations were conducted using Gaussian 09 program package. Geometry optimizations were conducted by DFT using Becke's three parameter exchange functional, and includes a corrected correlation functional of Lee, Yang, and Parr (LYP) with basis set 6-31G for FAP and PAP molecules [37]. In order to calculate the Fukui functions, the electron populations were calculated and performed at the optimized geometries of the neutral forms. All the calculations were calculated using of the ChemOffice program. The quantum chemical parameters, such as highest occupied molecular orbital (HOMO), lowest unoccupied molecular orbital (LUMO), energy gap (ΔE), ionization energy (I), absolute electronegativity (χ), softness (σ), hardness (η), dipole moment (μ), and fraction of electron transfer (ΔN), for the synthesized inhibitors (FAP and PAP) in the gas and aqueous phases were obtained using DFT techniques. The geometrical parameters can be calculated according to Equations (23-27) [38]:

$$\Delta E = E_{HOMO} - E_{LUMO} \quad (23)$$

$$\eta = -\frac{E_{HOMO} - E_{LUMO}}{2} \quad (24)$$

$$\sigma = \frac{1}{\eta} \quad (25)$$

$$\chi = -\frac{E_{HOMO} + E_{LUMO}}{2} \quad (26)$$

$$\Delta N = \frac{\phi - \chi_{inh}}{2(\eta_{Fe} + \eta_{inh})} \quad (27)$$

where χ_{Fe} is the iron electronegativity, χ_{inh} is the inhibitor electronegativity, η_{Fe} is the iron hardness, and η_{inh} is the inhibitor hardness. The ϕ value obtained from DFT calculations are 4.82 eV for Fe surface, and the computational value of hardness for iron was zero.

3. Results and discussion

3.1 Gravimetric Studies

Figs. 2 and 3 illustrate the change in the rate of corrosion and protection efficiency with varying concentrations of FRP and PRP in a 1 M HCl environment at 303 K. These statistics show that the rate of corrosion was highest in the uninhibited acidic media, but greatly diminished when the inhibitor was added. The mild steel coupons corroded at a corrosion rate of 5.37 mm/year without addition of an inhibitor, but this was reduced to 0.462 and 0.403 mm/year after 5 hours of immersion with 0.0005 M FRP and 0.0005 M PRP, respectively. Protection efficiencies of 93.3% and 96.5% were obtained with 0.0005 M FRP and 0.0005 M PRP, respectively.

This finding could be attributed to adsorption inhibitor molecules blocking corroded surface area, causing the rate of corrosion to be slowed [39]. The effect of FRP and PRP, appears to be a function of concentration. With an increasing concentration of FRP and PRP, the rate of corrosion falls, while the inhibition efficiency increases. This could be due to more surface covering [40].

3.2 Effect of 4-aminoantipyrine Derivative Structure on Protection Performance

The number of adsorption sites, their charge density, molecular size, and method of contact with the mild surface are all determined by the functional groups and structure of the inhibitor molecules. FRP and PRP are both 4-aminoantipyrine derivatives. They differ solely in their heterocyclic ring molecular structures, which are furan (five-member ring with an oxygen atom) for FRP and pyridine for PRP (six-member ring with a nitrogen atom). PRP's inhibitory ability is always stronger than FRP's in the experimental portion, at the same dosage and temperature. According to gravimetric measurements, PRP's at highest concentration has the maximum protection. Clearly, the nature of the heterocyclic ring influences its inhibitory effects. The electron density at the hetero atom (oxygen or nitrogen) is affected by the inhibitor molecule, which has an impact on

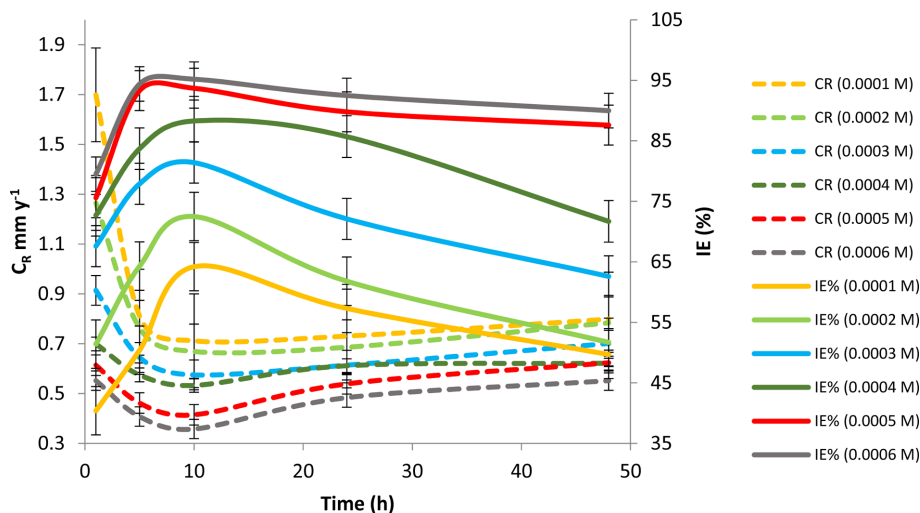


Fig. 2. Gravimetric curves of mild steel in 1 M HCl with different concentrations of FRP for various immersion times at 303 K

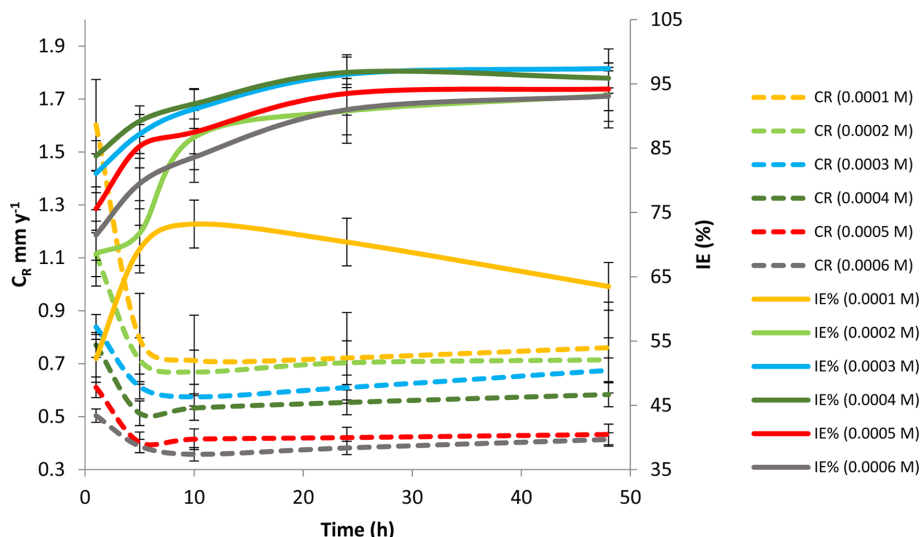


Fig. 3. Gravimetric curves of mild steel in 1 M HCl with different concentrations of PRP for various immersion times at 303 K

adsorption on the mild steel surface.

Heterocyclic aromatic rings are a crucial structural element in FRP and PRP molecules, because they increase electrostatic contact between inhibitors and mild steel surfaces. PRP is capable of building a strong bond with the mild steel surface in this regard. Furthermore, because of the pyridine ring, PRP is thought to provide better coverage. As a result, it outperforms FRP in terms of inhibition efficacy, 96.5%, c.f. 93.3% for FRP at 303 K.

3.3 Exposure Time Effect

Gravimetric tests were carried out for a prolonged period of 1 to 48 hours in the presence of optimum concentrations of FRP and PRP at 300 K to obtain more information about the inhibitors' stability and, as a result, their long-term effect on

corrosion inhibition. The results are presented in Figs. 2 and 3. For both synthesized corrosion inhibitors FRP and PRP, the variation of corrosion rates and protection performance with exposure time followed the same pattern. For periods ranging from 1 to 10 hours, the corrosion rate of FRP decreased from 0.614 to 0.415 mm/y and the protection performance increased from 75.6 to 93.7%, while the rate of corrosion of PRP reduced from 0.611 to 0.415 mm/y and the rate increased from 90.8 to 96.8%.

With increasing exposure duration, the absorptive coating on the mild steel surface becomes stronger. Due to the delayed desorption of inhibitor molecules, a modest drop in inhibitor efficiency was seen after a 24-hour period. The stability of FRP and PRP in 1M HCl was proven over a longer exposure period.

Table 1. Compares reported corrosion inhibitors to the one under investigation

Corrosion inhibitor.	Metal	Acid	IE%	Ref.
4-((furan-2-ylmethylene)amino)antipyrine (FAP)	Mild steel	HCl	93.3	-
4-((pyridin-2-ylmethylene)amino)antipyrine (PAP)	Mild steel	HCl	96.5	-
3-(4-ethyl-5-mercapto-1, 2, 4-triazol-3-yl)-1-phenylpropanone (EMTP)	Mild steel	HCl	97	41
2-(4-phenyl-1H-1,2,3-triazol-1-yl) acetohydrazide	Mild steel	HCl	95.3	42
2-Amino-4-phenyl-N-benzylidene-5-(1,2,4-triazol-1-yl)thiazole	Mild steel	HCl	95	42
7-((1-benzyl-1H-1,2,3-triazol-4-yl)methyl)-1,3-dimethyl-3,7-dihydro-1H-purine-2,6-dione	Mild steel	HCl	91.7	43
7-((1-(4-fluorobenzyl)-1H-1,2,3-triazol-4-yl)methyl)-1,3-dimethyl-3,7-dihydro-1H-purine-2,6-dione	Mild steel	HCl	86.9	43
7-((1-(4-chlorobenzyl)-1H-1,2,3-triazol-4-yl)methyl)-1,3-dimethyl-3,7-dihydro-1H-purine-2,6-dione	Mild steel	HCl	94	43
7-((1-(4-bromobenzyl)-1H-1,2,3-triazol-4-yl)methyl)-1,3-dimethyl-3,7-dihydro-1H-purine-2,6-dione	Mild steel	HCl	91.8	43
7-((1-(4-iodobenzyl)-1H-1,2,3-triazol-4-yl)methyl)-1,3-dimethyl-3,7-dihydro-1H-purine-2,6-dione	Mild steel	HCl	90.9	43
5-methyl-4-((3-nitrobenzylidene) amino) -2,4-dihydro- 3H-1,2,4-triazole-3-thione	Mild steel	HCl	89.7	44
3-phenyl-4-amino-5-mercapto-1,2,4-triazole	Mild steel	HCl	97	45
2[5-(2-Pyridyl)-1,2,4-triazol-3-yl phenol	Mild steel	HCl	96.8	46
3,5-Bis(4-methyltiophenyl)-4H-1,2,4-triazole	Mild steel	HCl	93.5	46
3,5-Bis(4-pyridyl)-4H-1,2,4-triazole	Mild steel	HCl	89.1	46
3,5-Diphenyl-4H-1,2,4-triazole	Mild steel	HCl	82.8	47
3,5-Di(<i>m</i> -tolyl)-4-amino-1,2,4-triazole	Mild steel	HCl	95.8	48
5-Amino-1,2,4-triazole	Mild steel	HCl	24	48
5-Amino-3-mercapto-1,2,4-triazole	Mild steel	HCl	82	48
5-Amino-3-methyl thio-1,2,4-triazole	Mild steel	HCl	82	48
1-Amino-3-methyl thio-1,2,4-triazole	Mild steel	HCl	63	49
3-Benzylidene amino-1,2,4-triazole phosphonate	Mild steel	HCl	56.9	49
3- <i>p</i> -Nitro-benzylidene amino-1,2,4-triazole phosphonate	Mild steel	HCl	69.2	49
3-Salicylalidene amino-1,2,4-triazole phosphonate	Mild steel	HCl	43.2	49
3,5-Bis(methylene octadecyldimethylammonium chloride)-1,2,4-triazole	Mild steel	HCl	98.3	50
3-Amino-1,2,4-triazole-5-thiol	Mild steel	HCl	97.8	51

3.4 Effect of Temperature

The mild steel corrosion parameters in 1M HCl in the absence and presence of various concentrations of FRP or PRP have been determined utilizing gravimetric measurements. Gravimetric investigations were conducted at temperatures of 303, 313, 323, and 333 K to observe the influence of temperature, and the findings are shown in Figs. 4 and 5. In 1 M HCl solution, the results demonstrate that the inhibitor FRP or PRP acts as a strong corrosion inhibitor for mild steel, with protection efficacy being concentration and temperature dependent. Increases in FRP or PRP concentration produce an increase in inhibition efficiency, which peaks at 93.7 % at 0.0005 M at 303 K. Further increases in FRP concentration resulted in a less noticeable increase in protection efficacy (95.2 %), due to desorption of part of the FRP molecules.

Over the concentration range examined, the inhibition efficacy of FRP or PRP is higher than that of some organic inhibitors described in the literature [41-51], see Table 1. In comparison to previously researched organic compound-based corrosion inhibitors, the current inhibitors FRP and PRP exhibit significantly greater inhibition efficacy at very low concentrations.

Increased temperature caused a reduction in inhibitory efficacy at all concentrations investigated, implying physical adsorption. At elevated temperatures, the existing weak Vander Waal's forces tend to reduce in this form of adsorption [52]. Figs. 4 and 5 show the corrosion inhibition behavior of FRP or PRP at temperatures ranging from 303 to 333 K in the presence of various inhibitor concentrations and a 5-hour immersion time. At the temperatures examined (323 and 333 K), the presence

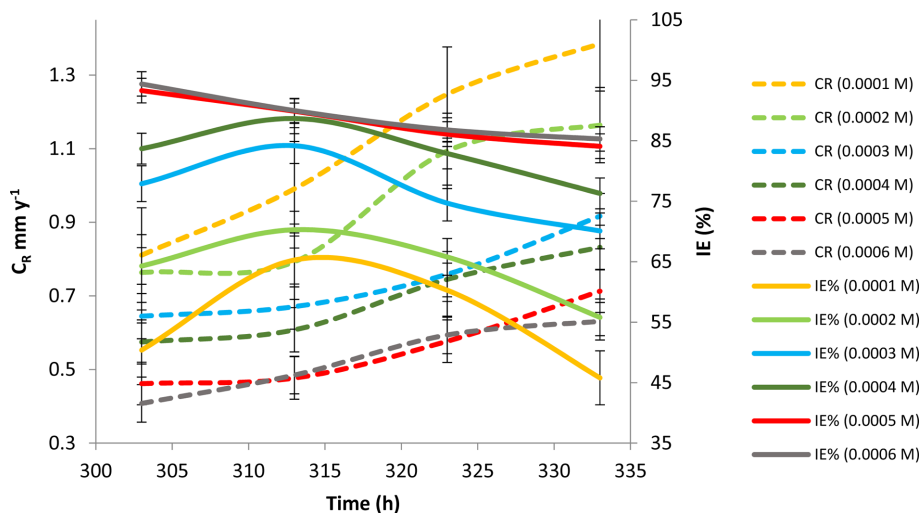


Fig. 4. Relationship between corrosion rate / inhibition efficiency and concentration of FRP at various temperatures for 5h immersion time

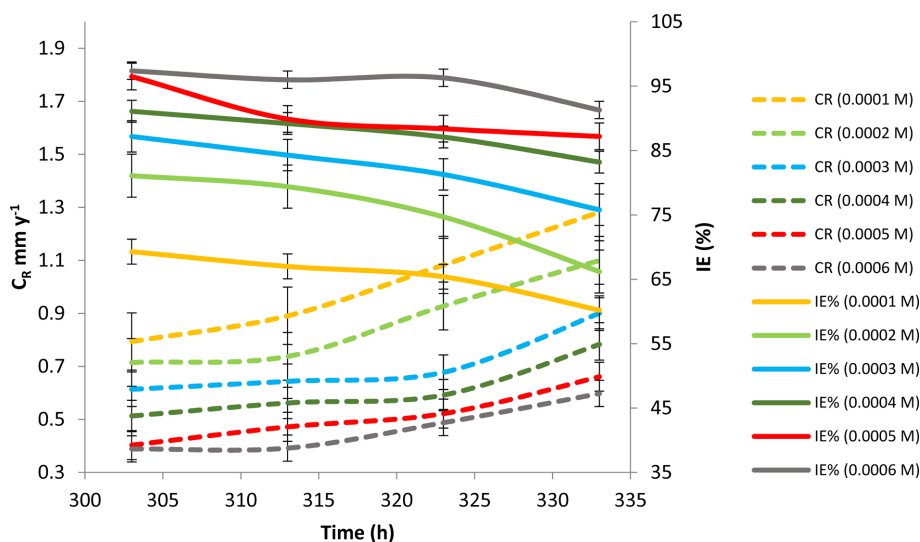


Fig. 5. Relationship between corrosion rate / inhibition efficiency and concentration of PRP at various temperatures for 5h immersion time

of varied inhibitor concentrations of FRP or PRP reduced the inhibition efficacy marginally. For FRP, the highest protection efficacy was 93.3% at 0.0005 M at 303 K, but it reduced to 84.1% at 333 K. For PRP, the maximum inhibition efficiency was 96.5% at 0.0005 M at 303 K, but it reduced to 87.2% at 333 K for a 5 h immersion duration. Figs 4 and 5 show a modest decrease in inhibitory efficacy with increasing temperature, which points to a physical adsorption process [53].

Finally, the influence of temperature on corrosion rate and inhibition efficiency was investigated in 1 M HCl at temperatures ranging from 303 to 333 K in the presence and absence of various inhibitor doses (5h immersion time). The inhibition efficiency of both tested inhibitors was observed to

decrease somewhat as the temperature was raised from 303 to 333 K. Desorption of adsorbed inhibitor molecules on the gentle surface could explain this. This demonstrates that inhibition occurs due to inhibitor adsorption on the metal surface, with desorption facilitated by increasing temperature. Figs 4 and 5 indicate that the inhibitory efficiency of FRP and PRP drop marginally as the temperature rises. This can be explained by chemical adsorption of FRP and PRP on the mild steel surface.

3.5 Adsorption Isotherms

Adsorption isotherms can provide essential data on the interaction between inhibitor molecules and mild steel surfaces. Two types of adsorption isotherm are advocated for this method.

In the current work, we applied the adsorption mechanism of synthesized tested inhibitors FRP and PRP using Temkin and Langmuir adsorption isotherms [54].

The adsorption isotherm could be used to visualize and study the inhibitor-metal surface interactions. The adsorption mechanism of inhibitors can indeed be described using both forms of interaction: physical adsorption and chemical adsorption [55]. These processes are influenced by the inhibitor molecules' chemical structures, experimental temperature, redox potential, charges, and metallic characteristics. Adsorption of organic inhibitor molecules from aqueous solutions is thought to be a quasi-substitution process between organic compounds in the aqueous phase [Org(sol)] and water molecules connected to the metal substrate [$H_2O_{(ads)}$], as shown by the equilibrium (Equation (1)) [56]:



where x is the number of water molecules that have been substituted by a single chemical molecule. In this scenario, the adsorption of FAP and PAP is followed by the release of water molecules from the steel surface.

Several isotherm models including Langmuir, and Temkin, adsorption isotherm models [51] are used to create an acceptable adsorption behavior for FAP and PAP adsorption on metallic surfaces. The graphs of percentage surface coverage (C_{inh}/θ) versus inhibitor concentrations (C_{inh}) at various temperatures were used to assess the better adsorption isotherms (Langmuir or Temkin kind) of FAP and PAP. As seen in Figs. 6 and 7, straight lines with almost unit slopes have been obtained, indicating that the adsorption of the studied inhibitors on the steel surface obeyed the Langmuir model.

The Langmuir model is shown in Equation (2) [57]:

$$\frac{C}{\theta} = \frac{1}{K} + C \quad (2)$$

where, K refers to the adsorption equilibrium, and θ represents the surface coverage value and can be calculated according to Equation (3):

$$\theta = \frac{IE}{100} \quad (3)$$

The correlation coefficient (R^2) is used to determine if the adsorption isotherm model matches the experimental data [58]. Figs. 6 and 7 show the application of Langmuir adsorption for assessment. The correlation coefficients for the straight lines between C and C/θ are close to 1, and the slope values in the Langmuir equation are nearly equal to 1. The Langmuir adsorption isotherm governs the adsorption of FRP and PRP on the mild steel surface, and each FRP or PRP molecule only contributes for one adsorption position.

Moreover, we also suggested to use Temkin adsorption

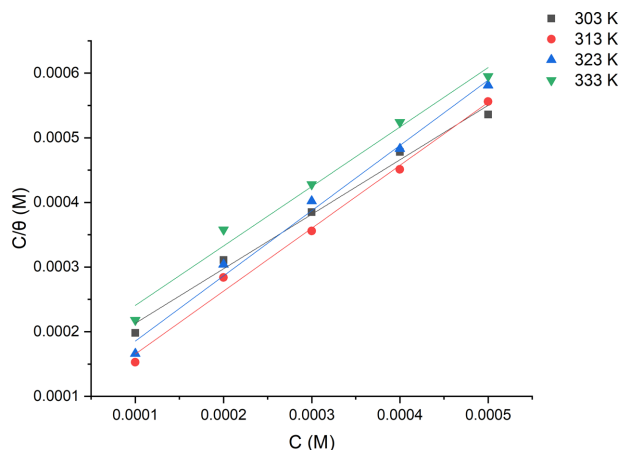


Fig. 6. Langmuir's adsorption isotherms of FRP in 1.0 M HCl

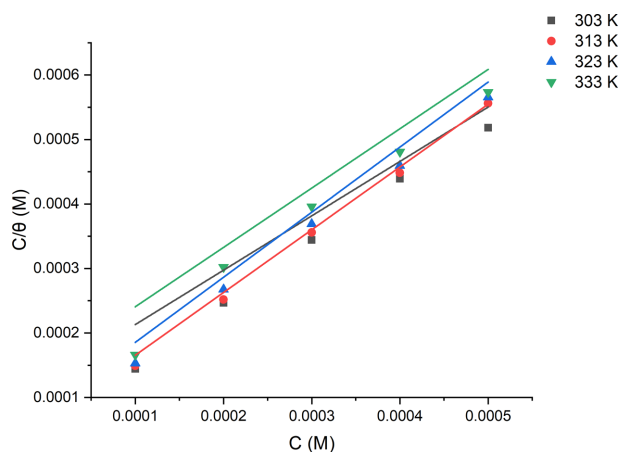


Fig. 7. Langmuir's adsorption isotherms of PRP in 1.0 M HCl

isotherm in addition to Langmuir adsorption isotherm in order to study the adsorption mechanisms of 4-aminoantipyrine derivatives.

Temkin equation is presented in Equation (4)

$$\ln K.C = a.\theta \quad (4)$$

where, a refers to the interaction in the adsorption.

Based on Figs. 8 and 9, the plots between $\ln C$ against θ are significantly vary from unit. They confirm that adsorption of FRP or PRP on the surface of mild steel do not obey the Temkin adsorption isotherm.

According to (K) values, the adsorption free energies of (ΔG°) for FRP and PRP molecules were determined by Equation (5):

$$\Delta G^\circ = -RT \ln(55.5 K) \quad (5)$$

where R represents the universal gas constant ($R = 8.314 J$

$\text{mol}^{-1}\text{K}^{-1}$), and T refers to the solution temperature (K).

Furthermore, the value of ΔG° offers a lot of information. ΔG° is greater than -20 kJ mol^{-1} , indicating that the charged inhibitors and charged steel interact electrostatically (physical

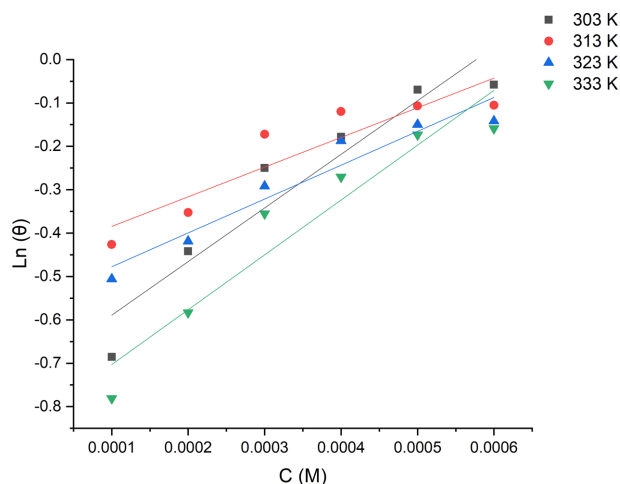


Fig. 8. Temkin's adsorption isotherms of PRP in 1.0 M HCl

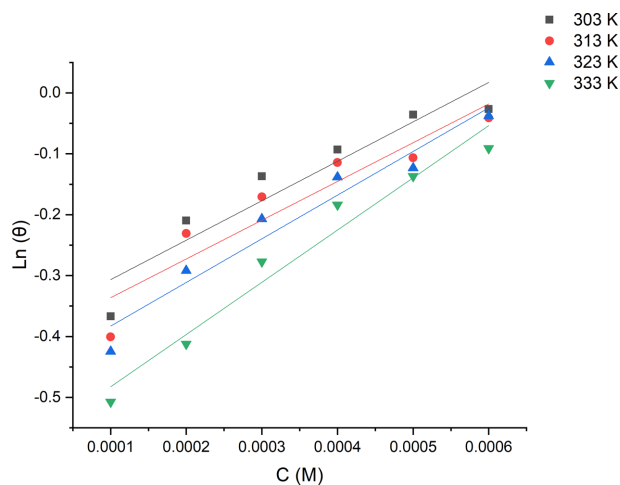


Fig. 9. Temkin's adsorption isotherms of PRP in 1.0 M HCl

adsorption). While the adsorption entails the transfer of a charged pair of organic inhibitors onto the steel surface, resulting in the formation of a type of coordinated bonds (chemical adsorption) while it is more negative than -40 kJ mol^{-1} [59]. There is no distinction between physical and chemical adsorption, with the former being the first stage of chemical adsorption. When examining the value of ΔG° , the adsorption of FPR ($\Delta G^\circ = -37.63 \text{ kJ mol}^{-1}$) and PRP ($\Delta G^\circ = -34.88 \text{ kJ mol}^{-1}$) on mild steel surfaces is a mixture of both physisorption and chemisorption. The ΔG° value becomes increasingly negative as the temperature rises, suggesting that the investigated inhibitors are more tightly bound to the steel surface.

2.6. An investigation of the mild steel surface

SEM technique was used to examine the surface characteristics of mild steel specimens in the absence and presence of tested inhibitors. Fig. 10(a, b, and c) depicts the modifications that observed in the mild steel specimens. Mild steel surface in 1 M HCl is shown in Fig. 10(a). The mild steel surface in 1 M HCl containing FAP and PAP are shown in Fig. 10(b) and Fig. 10(c) respectively. The smooth surface of the Fig. 10(b) and Fig. 10(c) exhibited in Fig. 10(b and c) were attributable to the inhibitor molecules adsorbing on the surface.

3.6 Computational studies

Several computational chemistry methods, including density functional theory (DFT), molecular dynamics (MD), and Monte Carlo (MC) simulations, have recently emerged as powerful corrosion monitoring tools [60]. DFT simulations are the most powerful computational tool, providing vital indices such as the energy of frontier molecular orbitals (FMOs), EHOMO and ELUMO, and numerous correlation parameters such as energy band gap ($E_{\text{LUMO}} - E_{\text{HOMO}} = \Delta E$), hardness (η), electronegativity (χ), dipole moment (μ), softness (σ), fraction of electron transfer (ΔN) and so on, with which the adsorption ability and corrosion inhibition effectiveness of a compound can be evaluated. DFT studies are commonly used to correlate the relative inhibitory effect of a group of drugs with comparable molecular structures.

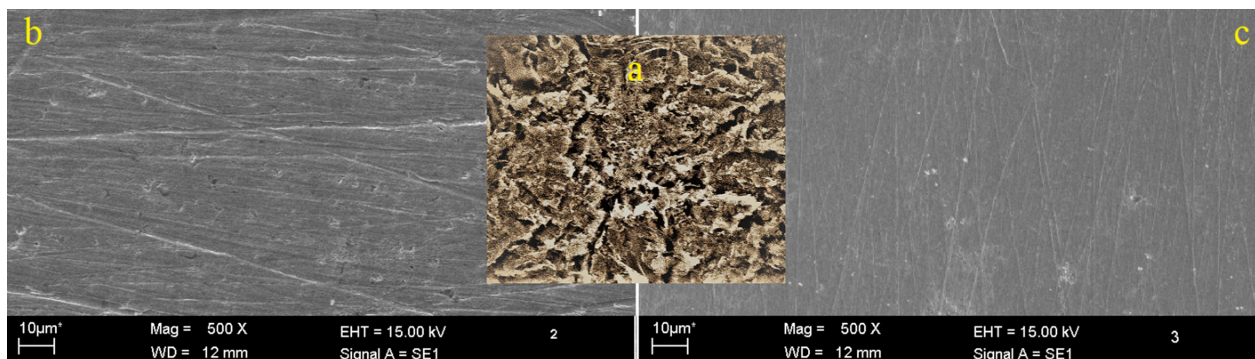


Fig. 10. SEM pictures of mild steel (a) with a 1 M HCl solution, and (b) with a 1 M HCl solution containing FAP, and (c) with a 1 M HCl solution containing PAP

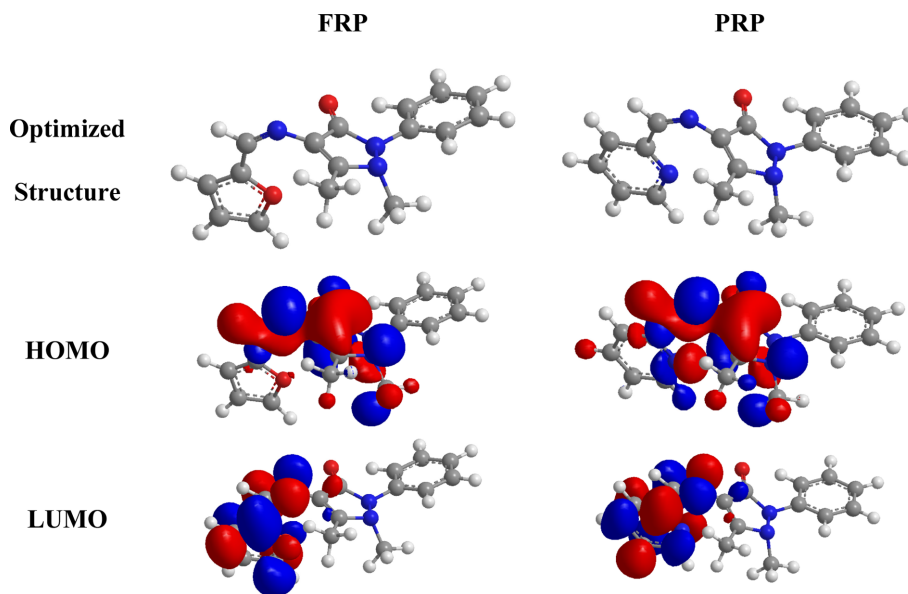


Fig. 11. Optimized structures, HOMO and LUMO for the tested inhibitors at B3LYP/6-311G(d,p) in the gas phase

In general, higher E_{HOMO} , softness (σ) and dipole moment (μ) and lower E_{LUMO} , ΔE , electronegativity (χ) and hardness (η) values are associated with high inhibition efficiency [61].

The energy band gap E ($E_{\text{LUMO}} - E_{\text{HOMO}}$) is one of the most important indices, and a lower value is related with a better inhibitory efficiency. It is necessary to note that the iron atoms on the mild steel surface and inhibitor molecules interactions heteroatoms and/or pi-bonds, of the inhibitor molecules are affected in bonding with the mild steel surface. These heteroatoms and/or pi-bonds are named adsorption or active centers.

The application of DFT is recognized as one of the most important ways for selecting the relevant sites of the inhibitor molecule among the various theoretical and experimental approaches [62]. The electron rich centers (active centers) that actively contribute to charge sharing with the metallic surface are represented by localized regions in FMOs (HOMO and LUMO). Aromatic ring(s) and/or polar functional groups are the most common electron-rich centers. The contribution of FMOs in charge sharing with the metal surfaces, on the other hand, is highly dependent on the type of the substituents.

For studying the structure and behavior of corrosion inhibitors, the quantum chemistry technique is highly beneficial [63]. Several thermodynamic parameters may be estimated computationally from Gaussian output files based on the optimized structures of FRP and PRP at B3LYP/6-311G(d,p), Fig. 11. Mulliken charges are used to estimate inhibitor adsorption centers. Because they are more negatively charged, the oxygen and nitrogen atoms in FRP and PRP are the most favourable sites for adsorption of these inhibitors onto the metal surface via a donor–acceptor type of interaction, as shown in Table 2. Furthermore, in FRP and PRP, the heterocyclic and

benzene rings stimulate the formation of adsorbate–surface complexes [64].

The electron-donating location of the molecule can be displayed using the highest occupied molecular orbital (HOMO) [65]. According to the HOMO diagrams of FRP and PRP in Fig. 11, both can donate electrons to the metal surface, primarily at the O and N atoms. The lowest unoccupied molecular orbital (LUMO), on the other hand, reflects the compound's ability to receive electrons. The shapes of the LUMOs in Fig. 11 demonstrate that the FRP and PRP receiving positions are comparable. Nitrogen, oxygen, and carbon atoms are perhaps the most active LUMO centers in FRP and PRP (near the double bonds or heterocyclic ring). When looking at the HOMO values in Table 2, it's evident that PAP, which has the highest inhibitory efficiency, also has the highest E_{HOMO} as computed using the DFT/B3LYP/6-31G basis set for both gas and aqueous phases. As per the HOMO, the two explored Schiff bases are PAP > FAP; E_{HOMO} . This backs up the experimentally determined ranking. According to the DFT/B3LYP/6-31G computations, FAP has the highest LUMO value in the aqueous phase, while PAP and FAP have about identical LUMO values in the gas phase; thus, it has the lowest chance to interact with the mild steel surface. The variation in energy between the HOMO and the LUMO (E) is a significant element in determining chemical reactivity, kinetic stability, chemical hardness/softness, and optical polarizability of organic compounds. Large values of ΔE result in strong electrical stability and minimal reactivity. On the other hand, high values of E imply high reactivity since electrons are easily excited and transferred from the HOMO to the LUMO. As a result, lower E values indicate a good organic corrosion inhibitor. According to the DFT/B3LYP/6-31G

Table 2. Quantum Chemical Parameters for Inhibitors at B3LYP/6-311G(d,p)

Inhibitors	E_{HOMO} (eV)	E_{LUMO} (eV)	ΔE (eV)	χ (eV)	η (eV)	σ (eV ⁻¹)	ΔN
FRP (Gas)	-7.287	-2.915	4.372	5.101	2.186	0.457	-0.064
PRP (Gas)	-7.79	-3.149	4.641	5.469	2.320	0.431	-0.139
FRP (Aqueous)	-7.523	-3.142	-4.381	5.332	2.190	0.456	-0.116
PRP (Aqueous)	-8.435	-3.007	-5.428	5.721	2.714	0.368	-0.165

calculations, PAP has the lowest value of E in both gas and aqueous phases, indicating that it has the strongest response, along with FAP. On decreasing values of ΔN , which is an electron transfer from the Schiff bases to the mild steel surface that has also been computed, the efficiency of Schiff bases increases. The Schiff bases have ΔN values ($\Delta N < 0$). The quantum parameters energy of HOMO (E_{HOMO}), energy of LUMO (E_{LUMO}), energy gap ($\Delta E_{\text{L-H}}$), electronegativity (χ), hardness (η), softness (σ), and the number of electrons transferred (ΔN) are determined and listed in Table 2.

The E_{HOMO} value of a molecule is used to determine its ability to donate electrons. A molecule with a higher E_{HOMO} can easily donate electrons to low-energy, empty molecular orbital acceptor molecules. The E_{HOMO} value of FRP (-7.287 eV) is lower than the E_{HOMO} value of PRP (-7.79 eV) in Table 2, which is in line with the experimental data. The ability of a molecule to take electrons is represented by the E_{LUMO} value. The lower the E_{LUMO} 's value, the easier it is for it to accept electrons.

The inhibitory efficiency can be sorted in the following order: PRP > FRP, based on the computed E_{LUMO} values in Table 2.

The variation in chemical potential on the total number of atoms is represented by absolute hardness (η). The higher the absolute hardness of a compound's stability, the more stable it is. PRP has a higher inhibitory efficiency than FRP, based on the computed values in Table 2. Furthermore, PRP has a higher ΔN value than FRP. It also suggests that PRP has a stronger ability to exchange electrons than FRP. In summary, the quantum chemical parameters (E_{LUMO} , ΔE , η , σ , and ΔN) of neutral inhibitors correspond well with the above-mentioned experimental data. It is important to note that both PRP and FRP are studied in acid solution.

3.7 Mulliken charges

Mulliken charges are used to determine the adsorption centers of the tested inhibitor. The easier it is for the atoms to transfer electrons, the more negatively charged they are. Table 3 shows that the N, and O atoms are electron-donating sites in the inhibitor compounds that have been studied. It is obvious from Table 3, that O(3), and N(4), have the highest atomic charges. These atoms have the ability to bonded with the metal surface

Table 3. Mulliken atomic charges of FRP and PRP in the gas phase

FRP						PRP					
No.	Charge										
C1	-0.1383	C8	-0.171	N15	-0.1025	C1	-0.1275	C8	-0.1759	C16	0.0136
C2	0.3328	C9	0.0617	C16	0.0415	C2	0.3417	C10	-0.1343	C17	-0.0357
O3	-0.303	C10	-0.1403	O17	-0.087	O3	-0.3159	C11	-0.1142	C18	-0.1544
N4	-0.2017	C11	-0.1143	C18	-0.0873	N4	-0.2318	C12	-0.1487	C19	-0.0948
N5	-0.0904	C12	-0.1471	C19	-0.1423	N5	-0.0776	C13	-0.1168	C20	-0.1674
C6	-0.1314	C13	-0.1181	C20	-0.2081	C6	-0.1349	C14	-0.1609	C21	-0.0646
C7	-0.0109	C14	-0.1556	C21	-0.0683	C7	0.0174	N15	-0.1157	N22	-0.1154

and forming coordination bonds.

3.8 Fukui Functions

To use the Mulliken population analysis, the nucleophilic sites (f_k^+), electrophilic sites (f_k^-), and the dual descriptor ($\Delta f(k)$) were computed by applying relations (6-8),

$$f_k^+ = q_k(N+1) - q_k(N) \quad (6)$$

$$f_k^- = q_k(N) - q_k(N-1) \quad (7)$$

$$\Delta f(k) = f_k^+ - f_k^- \quad (8)$$

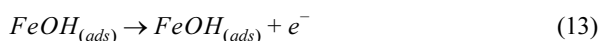
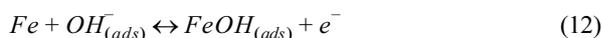
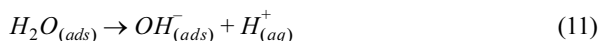
where q_k is the atomic charge in its neutral (N), cationic (N - 1), or anionic (N + 1) state.

The Fukui data for the Schiff bases (FAP, and PAP) are determined as a result of the Fukui analysis.

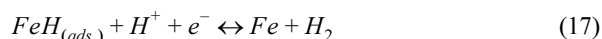
The oxygen atom of the carbonyl group, which is directly linked to the heterocyclic ring, has the largest value of (f_k^-), with values of 0.116 (atomic charge = -0.303) and 0.131 (atomic charge = -0.3159) for FAP and PAP, respectively. (47) This implies that it has a strong ability to donate electrons to the surface of mild steel. The FAP and PAP molecules' nitrogen atoms have high values of (f_k^-) and participate in the donating process. We can get two indicators for both donor ($f(r) < 0$) and acceptor ($f(r) > 0$) sites using the dual descriptor ($\Delta f(k)$). The oxygen and nitrogen atoms are the optimum for donor sites, with values of -0.303 [O3], -0.2017 [N4] and -0.3159 [O3], -0.2318 [N4] for FAP and PAP, respectively. The optimum acceptor site for both FAP and PAP is the carbon atom, which has an atomic charge value of -0.1314 and -0.1349 for FAP and PAP, respectively.

3.9 Corrosion and Corrosion Inhibition Mechanisms

Mild steel corrosion in HCl solution is primarily uniform corrosion. When a mild steel sample is dipped in an HCl environment, an attack on the mild steel occurs due to the creation of ferrous ionic species (Fe^{2+}) and the generation of hydrogen. The steps that followed have been used to describe this mechanism, [66]. The following equations show how anodic dissolution works. (9) to (14):



In addition, the following equations determine cathodic H_2 development (15) to (17):



Regrettably, the mechanism of the inhibition technique by the investigated Schiff bases was explained in terms of the adsorption of the Schiff bases molecules at the metal/solution interface, based on the available findings obtained from the gravimetric methods, which indicated that the evaluated Schiff bases behave as proficient inhibitors for the corrosion of mild steel in 1.0 M HCl solution, and also the earlier described investigations. Physical, chemical, or a combination of the two adsorption mechanisms could be used in the adsorption process. The current report's thermodynamic parameters indicated that the nature of the two inhibitors' adsorption on the mild steel surface in HCl solution was mostly physically and chemically. The inhibitor molecules' adsorption on the mild steel surface was determined by their chemical compositions, the strength of charge density, and the acidic environment's nature. The chemical compositions of the investigated Schiff bases molecules (Fig. 1) demonstrate that they exhibit a variety of adsorption mechanisms, which can be characterized as follows:

First, sections of the Schiff bases molecules were protonated in an acidic solution [67], resulting in protonated cations coexisting with neutral Schiff bases molecules.

Electrostatic interaction between the protonated inhibitor molecules and the positively charged mild steel surface is based on consideration. Conversely, in HCl environment, the originally adsorbed negatively charged chloride anions (Cl^-) are

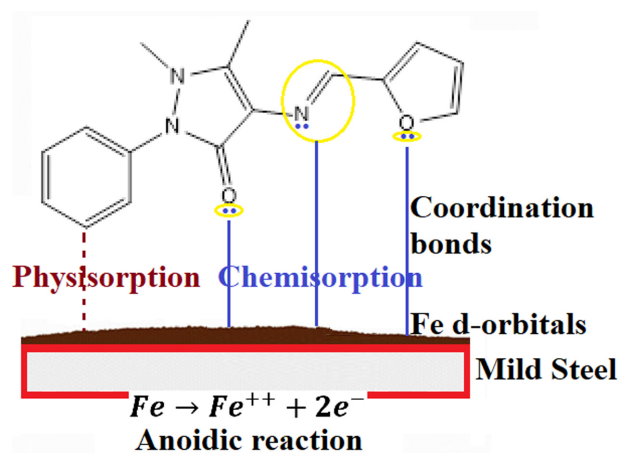


Fig. 12. The adsorption mechanism of FAP molecules on the mild steel surface

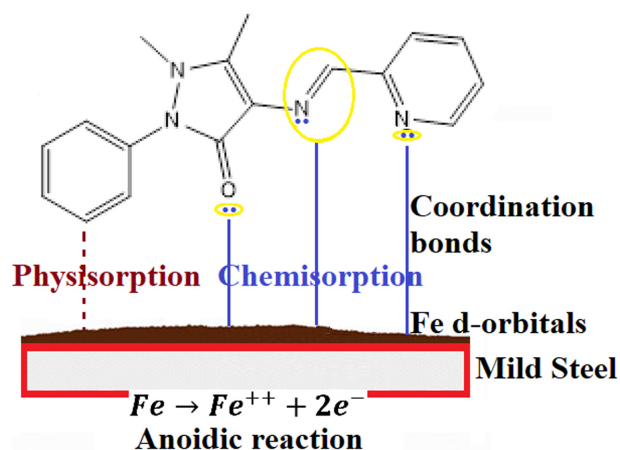
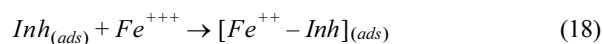


Fig. 13. The adsorption mechanism of PAP molecules on the mild steel surface

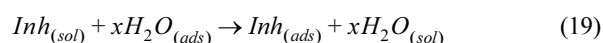
extended to meet the positive charges steel surface, resulting in an excessive negative charge on the steel surface. As a result of the electrostatic attraction between the negatively charged surface and the protonated inhibitor molecules, a protective barrier will form on its surface (physical adsorption).

Secondly, the creation of coordination bonds between the lone pairs of electrons positioned on the oxygen and nitrogen in Schiff bases molecules, and the unoccupied d-orbitals of Fe atoms, may result in adsorption of the Schiff bases molecules (Figs. 12 and 13).

Furthermore, π -electrons in the aromatic rings of the investigated Schiff bases molecules can adsorb via a donor-acceptor interaction (chemical adsorption) [68]. Third, the dye compounds studied are excellent ligands that can form coordination complexes by chelating with metal ions. As a result, they may form metal-inhibitor complexes $[Fe^{2+} - Inh]_{(ads)}$ with Fe^{2+} ions produced on the mild steel surface, forming a blocking barrier to further dissolution according to the equation below (18),



Adsorption of inhibitor molecules also necessitates the replacement of one or even more water molecules adsorbed on the surface of the metal by these same molecules or the anions of the acidic solutions, as shown in equation (19),



Eventually, iron oxidizes in hydrochloric acid solution, forming ferrous salt ($FeCl_2$) with the release of $H_2 \uparrow$, as explained by the equation below (20), [69-72]



The $FeCl_2$ generated is less soluble and clings tightly to the mild steel surface, forming a protecting layer that protects the mild steel surface from additional HCl attack.

4. Application

Corrosion inhibitors are typically applied in oil and gas production to mitigate corrosion caused by the presence of acidic gases. The laboratory testing performed when evaluating corrosion inhibitors normally only assesses inhibitor efficacy in preventing general corrosion. Unfortunately, there are still a number of difficulties to consider in the established uses of corrosion inhibitors, such as pricing, degradability, and thermal stability, to name a few [73]. Besides the use of Schiff bases derived from 4-aminoantipyrine in coordination chemistry, they are extensively used in the fields like corrosion inhibition, energy harvesting, antimicrobial, anti-inflammatory, antioxidant, cytotoxicity, anti-convulsant, anthelmintic activity, analgesic, antipyretic, DNA binding and DNA cleavage, etc.

5. Conclusions

The use of corrosion inhibitors is one of the significant techniques for mild steel surface modification to control or impede the corrosion. In the current investigation, the Schiff bases derived from 4-aminoantipyrine namely 4-((furan-2-ylmethylene)amino)antipyrine (FAP) and 4-((pyridin-2-ylmethylene)amino)antipyrine (PAP) were successfully synthesized and fully characterized. For the corrosion inhibition investigation, the potential of FRP and PRP to suppress corrosion has been studied using gravimetric measurements and quantum chemical calculations. The influence of molecular structure, concentration, immersion time, and temperature on corrosion inhibition has been examined. The following are the most important conclusions:

1. FRP and PRP are prospective mild steel corrosion inhibitors in 1 M HCl, with efficiencies at 303 K of 93.3 % and 96.5%, respectively. Because PRP has a pyridine ring in its structure, it has a better inhibitory ability than FRP in the same conditions.
2. As the inhibitor concentration rises, the inhibition efficacy rises, and the inhibitors tend to be more tightly coupled to the mild steel surface.
3. The adsorption of FRP and PRP on the mild steel surface is consistent with Langmuir adsorption, which is a combination of physical and chemical adsorption.
4. Although there have been few reports that molecular adsorption orientation can be detected by improved electron microscopic technology [71,72], the interface adsorption behavior of many corrosion inhibitors cannot be directly observed from experimental perspective. In this work, we focus on a cheap organic small molecule (FRP and PRP), and its inhibition effect on mild steel corrosion in 1 M HCl were fully

investigated by a series of experimental and theoretical methods. SEM morphology observations prove the film-forming capability of the FRP and PRP molecules over the mild steel surface.

5. Computation analyses were used to estimate the ability of FRP and PRP to suppress corrosion. As a result, both experimental and theoretical results are in good accord.

6. Overall, our findings suggest that FRP and PRP are nontoxic, highly soluble, and effective corrosion inhibitors. It is of great significance for enhancing the corrosion resistance of steel surfaces

Acknowledgments

The authors are grateful to the Universiti Kebangsaan Malaysia (UKM) for support under project code: GUP-2020-012.

References

1. F. Bentiss, F. Gassama, D. Barbry, L. Gengembre, H. Vezin, M. Lagrenée, M. Traisnel, Enhanced corrosion resistance of mild steel in molar hydrochloric acid solution by 1, 4-bis (2-pyridyl)-5H-pyridazino [4, 5-b]indole: Electrochemical, theoretical and XPS studies, *Applied Surface Science*, **252**, 2684 (2006). Doi: <https://doi.org/10.1016/j.apsusc.2005.03.231>
2. H. Lgaz, S. K. Saha, A. Chaouiki, K. S. Bhat, R. Salghi, P. Banerjee, I. H. Ali, M. I. Khan, I.-M. Chung, Exploring the potential role of pyrazoline derivatives in corrosion inhibition of mild steel in hydrochloric acid solution: Insights from experimental and computational studies, *Construction and Building Materials*, **233**, 117320 (2020). Doi: <https://doi.org/10.1016/j.conbuildmat.2019.117320>
3. Ehsani, A.; Nasrollahzadeh, M.; Mahjani, M.G.; Moshrefi, R.; Mostaanzadeh, H. Electrochemical and quantum chemical investigation of inhibitory of 1,4-Ph(OX)₂(Ts)₂ on corrosion of 1005 aluminum alloy in acidic medium, *Journal of Industrial And Engineering Chemistry*, **20**, 4363 (2014).
4. A. Dehghani, G. Bahlakeh, B. Ramezanzadeh, M. Ramezanzadeh, Detailed macro-/micro-scale exploration of the excellent active corrosion inhibition of a novel environmentally friendly green inhibitor for carbon steel in acidic environments, *Journal of the Taiwan Institute of Chemical Engineeris*, **100**, 239 (2019). Doi: <https://doi.org/10.1016/j.jtice.2019.04.002>
5. Asadi, N.; Ramezanzadeh, M.; Bahlakeh, G.; Ramezanzadeh, B. Utilizing Lemon Balm extract as an effective green corrosion inhibitor for mild steel in 1M HCl solution: A detailed experimental, molecular dynamics, Monte Carlo and quantum mechanics study, *Journal of the Taiwan Institute of Chemical Engineers*, **95**, 252 (2019). Doi: <https://doi.org/10.1016/j.jtice.2018.07.011>
6. H. Jafari, K. Sayin, Sulfur Containing Compounds as Corrosion Inhibitors for Mild Steel in Hydrochloric Acid Solution, *Transactions of the Indian Institute of Metals*, **69**, 805 (2016). Doi: <https://doi.org/10.1007/s12666-015-0556-2>
7. A. K. Singh, E. E. Ebenso, M. A. Quraishi, Adsorption Behaviour of Cefapirin on Mild Steel in Hydrochloric Acid Solution, *International Journal of Electrochemical Science*, **7**, 2320 (2012). Doi: <https://doi.org/10.1016/j.ijecs.2012.07.011>
8. Y.-S. Choi, J.-J. Shim, J.-G. Kim, Effects of Cr, Cu, Ni and Ca on the corrosion behavior of low carbon steel in synthetic tap water, *Journal of Alloys and Compounds*, **391**, 162 (2005).
9. D. Li, Y. Feng, Z. Bai, J. Zhu, M. Zheng, Influence of temperature, chloride ions and chromium element on the electronic property of passive film formed on carbon steel in bicarbonate/carbonate buffer solution, *Electrochimica Acta*, **52**, 7877 (2007). Doi: <https://doi.org/10.1016/j.electacta.2007.06.059>
10. C. Liu, R. I. Revilla, Z. Liu, D. Zhang, X. Li, H. Terryn, Effect of inclusions modified by rare earth elements (Ce, La) on localized marine corrosion in Q460NH weathering steel, *Corrosion Science*, **129**, 82 (2017). Doi: <https://doi.org/10.1016/j.corsci.2017.10.001>
11. Q. Ma, Z. Tong, W. Wang, G. Dong, Fabricating robust and repairable superhydrophobic surface on carbon steel by nanosecond laser texturing for corrosion protection, *Applied Surface Science*, **455**, 748 (2018). Doi: <https://doi.org/10.1016/j.apsusc.2018.06.033>
12. T. V. Shibaeva, V. Laurinavichyute, G. Tsirlina, A. M. Arsenkin, K. V. Grigorovich, The effect of microstructure and non-metallic inclusions on corrosion behavior of low carbon steel in chloride containing solutions, *Corrosion Science*, **80**, 299 (2014). Doi: <https://doi.org/10.1016/j.corsci.2013.11.038>
13. Y. Wang, Z. Jiang, Z. Yao, H. Tang, Microstructure and corrosion resistance of ceramic coating on carbon steel prepared by plasma electrolytic oxidation, *Surface Coatings Technology*, **204**, 1685 (2010). Doi: <https://doi.org/10.1016/j.surfcoat.2009.10.023>
14. V. S. Brito, I. Bastos, H. Costa, Corrosion resistance and characterization of metallic coatings deposited by thermal

- spray on carbon steel, *Materials & Design* **41**, 282 (2012). Doi: <https://doi.org/10.1016/j.matdes.2012.05.008>
15. X. Chen, C. Chen, H. Xiao, F. Cheng, G. Zhang, G. Yi, Corrosion behavior of carbon nanotubes–Ni composite coating, *Surface and Coatings Technology*, **191**, 351 (2005). Doi: <https://doi.org/10.1016/j.surfcoat.2004.04.055>
 16. Y. Ye, Z. Liu, W. Liu, D. Zhang, H. Zhao, L. Wang, X. Li, Superhydrophobic oligoaniline-containing electroactive silica coating as pre-process coating for corrosion protection of carbon steel, *Chemical Engineering Journal*, **348**, 940 (2018). Doi: <https://doi.org/10.1016/j.cej.2018.02.053>
 17. N. A. Negm, N. G. Kandile, E. A. Badr, M. A. Mohamed, Gravimetric and electrochemical evaluation of environmentally friendly nonionic corrosion inhibitors for carbon steel in 1M HCl, *Corrosion Science*, **65**, 94 (2012). Doi: <https://doi.org/10.1016/j.corsci.2012.08.002>
 18. C. Verma, E. Ebenso, I. Bahadur, I. Obot, M. Quraishi, 5-(Phenylthio)-3H-pyrrole-4-carbonitriles as effective corrosion inhibitors for mild steel in 1 M HCl: Experimental and theoretical investigation, *Journal of Molecular Liquids*, **212**, 209 (2015). Doi: <https://doi.org/10.1016/j.molliq.2015.09.009>
 19. C. Verma, M. Quraishi, A. Singh, 2-Amino-5-nitro-4, 6-diarylcyclohex-1-ene-1, 3, 3-tricarbonitriles as new and effective corrosion inhibitors for mild steel in 1 M HCl: Experimental and theoretical studies, *Journal of Molecular Liquids*, **212**, 804 (2015). Doi: <https://doi.org/10.1016/j.molliq.2015.10.026>
 20. D. Daoud, T. Douadi, H. Hamani, S. Chafaa, M. Al-Noaimi, Corrosion inhibition of mild steel by two new S-heterocyclic compounds in 1 M HCl: Experimental and computational study, *Corrosion Science*, **94**, 21 (2015). Doi: <https://doi.org/10.1016/j.corsci.2015.01.025>
 21. R. M. Kubba, A. S. Alag, Experimental and Theoretical Evaluation of new Quinazolinone Derivative as Organic Corrosion Inhibitor for Carbon Steel in 1M HCl Solution, *International Journal of Science and Research (IJSR)*, **6**, 1832 (2017). Doi: <https://doi.org/10.21275/ART20174699>
 22. F. Bentiss, M. Lagrenee, M. Traisnel, J. Hornez, The corrosion inhibition of mild steel in acidic media by a new triazole derivative, *Corrosion Science*, **41**, 789 (1999). Doi: [https://doi.org/10.1016/S0010-938X\(98\)00153-X](https://doi.org/10.1016/S0010-938X(98)00153-X)
 23. R. Baskar, D. Kesavan, M. Gopiraman, K. Subramanian, Corrosion inhibition of mild steel in 1.0M hydrochloric acid medium by new photo-cross-linkable polymers, *Progress in Organic Coatings*, **77**, 836 (2014). Doi: <https://doi.org/10.1016/j.porgcoat.2014.01.013>
 24. C. Verma, L. O. Olasunkanmi, E. E. Ebenso, M. A. Quraishi, Substituents effect on corrosion inhibition performance of organic compounds in aggressive ionic solutions: A review, *Journal of Molecular Liquids*, **251**, 100 (2018). Doi: <https://doi.org/10.1016/j.molliq.2017.12.055>
 25. E. A. Flores, O. Olivares, N. V. Likhanova, M. A. Domínguez-Aguilar, N. Nava, D. Guzman-Lucero, M. Corrales, Sodium phthalamates as corrosion inhibitors for carbon steel in aqueous hydrochloric acid solution, *Corrosion Science*, **53**, 3899 (2011). Doi: <https://doi.org/10.1016/j.corsci.2011.07.023>
 26. A. Dehghani, F. Poshtiban, G. Bahlakeh, B. Ramezanzadeh, Fabrication of metal-organic based complex film based on trivalent samarium ions-[bis (phosphonomethyl) amino] methylphosphonic acid (ATMP) for effective corrosion inhibition of mild steel in simulated seawater, *Construction and Building Materials*, **239**, 117812 (2020). Doi: <https://doi.org/10.1016/j.conbuildmat.2019.117812>
 27. B. Lin, Y. Zuo, Corrosion inhibition of carboxylate inhibitors with different alkylene chain lengths on carbon steel in an alkaline solution, *RSC Advances*, **9**, 7065 (2019). Doi: <https://doi.org/10.1039/C8RA10083G>
 28. K. S. Bokati, C. Dehghanian, S. Yari, Corrosion inhibition of copper, mild steel and galvanically coupled copper-mild steel in artificial sea water in presence of 1H-benzotriazole, sodium molybdate and sodium phosphate, *Corrosion Science*, **126**, 272 (2017). Doi: <https://doi.org/10.1016/j.corsci.2017.07.009>
 29. M. Finšgar, J. Jackson, Application of corrosion inhibitors for steels in acidic media for the oil and gas industry: A review *Corrosion Science*, **86**, 17 (2014). Doi: <https://doi.org/10.1016/j.corsci.2014.04.044>
 30. I. B. Onyeachu, M. M. Solomon, S. A. Umoren, I. B. Obot, A. A. Sorour, Corrosion inhibition effect of a benzimidazole derivative on heat exchanger tubing materials during acid cleaning of multistage flash desalination plants, *Desalination*, **479**, 114283 (2020). Doi: <https://doi.org/10.1016/j.desal.2019.114283>
 31. C. R. Vinodkumar, P. K. Radhakrishnan, Complexes of yttrium and lanthanide perchlorates with 4-N-(2'-furfurylidene)aminoantipyrine, *Synthesis and Reactivity in Inorganic and Metal-Organic Chemistry*, **27**, 1347 (1997). Doi: <https://doi.org/10.1080/00945719708000162>
 32. TM0193-2016-SG, Laboratory Corrosion Testing of Met-

- als in Static Chemical Cleaning Solutions at Temperatures below 93 °C (200 °F), NACE International (2000).
33. L. Guo, J. Tan, S. Kaya, S. Leng, O. Li, F. Zhang, Multidimensional insights into the corrosion inhibition of 3,3- dithiodipropionic acid on Q235 steel in H₂SO₄ medium: A combined experimental and in silico investigation, *Journal of Colloid and Interface Science*, **570**, 116 (2020). Doi: <https://doi.org/10.1016/j.jcis.2020.03.001>
 34. B. M. Prasanna, B. M. Praveen, N. Hebbar, Inhibition study of mild steel corrosion in 1 M hydrochloric acid solution by 2-chloro 3-formyl quinoline, *International Journal of Industrial Chemistry*, **7**, 9 (2016). Doi: <https://doi.org/10.1007/s40090-015-0064-6>
 35. ASTM International, Standard Practice for Preparing, Cleaning, and Evaluating Corrosion Test, 1–9 (2011).
 36. Koopmans T. Ordering of wave functions and eigenenergies to the individual electrons of an atom, *Physica*, **1**, 104 (1933). Doi: [https://doi.org/10.1016/S0031-8914\(34\)90011-2](https://doi.org/10.1016/S0031-8914(34)90011-2)
 37. M. E. Mashuga, L. O. Olasunkanmi, E. E. Ebenso, Experimental and theoretical investigation of the inhibitory effect of new pyridazine derivatives for the corrosion of mild steel in 1 M HCl, *Journal of Molecular Structure*, **1136**, 127 (2017). Doi: <https://doi.org/10.1016/j.molstruc.2017.02.002>
 38. E. A. Muller, B. Pollard, H. A. Bechtel, P. van Blerkom, M. B. Raschke, Infrared vibrational nanocrystallography and nanoimaging, *Science Advances*, **2** e1601006 (2016). Doi: <https://doi.org/10.1126/sciadv.1601006>
 39. L. Liu, N. Wang, C. Zhu, X. Liu, Y. Zhu, P. Guo, L. Alfifil, X. Dong, D. Zhang, Y. Han, Direct imaging of atomically dispersed molybdenum that enables location of aluminum in the framework of zeolite ZSM-5, *Angewandte Chemie International Edition*, **59**, 819 (2020). Doi: <https://doi.org/10.1002/anie.201909834>
 40. Tamalmani, K.; Husin, H. Review on Corrosion Inhibitors for Oil and Gas Corrosion Issues, *Applied Sciences*, **10**, 3389 (2020). Doi: <https://doi.org/10.3390/app10103389>
 41. Alamiery, A. Corrosion inhibition effect of 2-N-phenyl-amino-5-(3-phenyl-3-oxo-1-propyl)-1, 3, 4-oxadiazole on mild steel in 1 M hydrochloric acid medium: Insight from gravimetric and DFT investigations, *Materials Science for Energy Technologies*, **4**, 398 (2021). Doi: <https://doi.org/10.1016/j.mset.2021.09.002>
 42. A. A. Alamiery, Anticorrosion effect of thiosemicarbazide derivative on mild steel in 1 M hydrochloric acid and 0.5 M sulfuric Acid: Gravimetric and theoretical studies, *Materials Science for Energy Technologies*, **4**, 263 (2021). Doi: <https://doi.org/10.1016/j.mset.2021.07.004>
 43. I. Aziz, I. Annon, M. H. Abdulkareem, M. M. Hanoon, M. H. Alkaabi, L. M. Shaker, A. A. Alamiery, W. N. R. Wan Isahak, and M. S. Takriff, Insights into Corrosion Inhibition Behavior of a 5-Mercapto-1, 2, 4-triazole Derivative for Mild Steel in Hydrochloric Acid Solution: Experimental and DFT Studies, *Lubricants*, **9**, 122 (2021). Doi: <https://doi.org/10.3390/lubricants9120122>
 44. A. Nahlé, R. Salim, F. El Hajjaji, M. R. Aouad, M. Mes-sali, E. Ech-Chihbi, B. Hammouti, M. Taleb, Novel triazole derivatives as ecological corrosion inhibitors for mild steel in 1.0 M HCl: Experimental & theoretical approach. *RSC Advances*, **11**, 4147 (2021). Doi: <https://doi.org/10.1039/D0RA09679B>
 45. A. Espinoza-Vázquez, F. J. Rodríguez-Gómez, I. K. Martínez-Cruz, D. Ángeles-Beltrán, Negrón-Silva, G.E.; M. Palomar-Pardavé, L. L. Romero, D. Pérez-Martínez, A. M. Navarrete-López, Adsorption and corrosion inhibition behaviour of new theophylline–triazole-based derivatives for steel in acidic medium, *Royal Society Open Science*, **6**, 181738 (2019). Doi: <https://doi.org/10.1098/rsos.181738>
 46. I. Merimi, R. Benkaddour, H. Lgaz, N. Rezki, M. Mes-sali, F. Jeffali, H. Oudda, B. Hammouti, Insights into corrosion inhibition behavior of a triazole derivative for mild steel in hydrochloric acid solution, *Materialstoday Proceedings*, **13**, 1008 (2019). Doi: <https://doi.org/10.1016/j.matpr.2019.04.066>
 47. L. Wang, M. J. Zhu, F. C. Yang, C. W. Gao, Study of a triazole derivative as corrosion inhibitor for mild steel in phosphoric acid solution, *International Journal of Corrosion*, **2012**, 573964 (2012). <https://doi.org/10.1155/2012/573964>
 48. F. Bentiss, M. Bouanis, B. Mernari, M. Traisnel, H. Vezin, M. Lagrenee, Understanding the adsorption of 4H-1, 2, 4-triazole derivatives on mild steel surface in molar hydrochloric acid, *Applied Surface Science*, **253**, 3696 (2007). Doi: <https://doi.org/10.1016/j.apsusc.2006.08.001>
 49. B. El Mehdi, B. Mernari, M. Traisnel, F. Bentiss, M. Lagrenee, Synthesis and comparative study of the inhibitive effect of some new triazole derivatives towards corrosion of mild steel in hydrochloric acid solution, *Materials Chemistry and Physics*, **77**, 489 (2003). Doi: [https://doi.org/10.1016/S0254-0584\(02\)00085-8](https://doi.org/10.1016/S0254-0584(02)00085-8)
 50. H. H. Hassan, E. Abdelghani, M. A. Amin, Inhibition of mild steel corrosion in hydrochloric acid solution by triazole derivatives: Part I. Polarization and EIS Studies,

- Electrochimica Acta*, **52**, 6359 (2007). Doi: <https://doi.org/10.1016/j.electacta.2007.04.046>
51. S. Ramesh, S. Rajeswari, Corrosion inhibition of mild steel in neutral aqueous solution by new triazole derivatives, *Electrochimica Acta*, **49**, 811 (2004). Doi: <https://doi.org/10.1016/j.electacta.2003.09.035>
 52. L. G. Qiu, A. J. Xie, Y. H. Shen, A novel triazole-based cationic gemini surfactant: Synthesis and effect on corrosion inhibition of carbon steel in hydrochloric acid, *Materials Chemistry and Physics*, **91**, 269 (2005). Doi: <https://doi.org/10.1016/j.matchemphys.2004.11.022>
 53. B. D. Mert, M. E. Mert, G. Kardaş, B. Yazıcı, Experimental and theoretical investigation of 3-amino-1, 2, 4-triazole-5-thiol as a corrosion inhibitor for carbon steel in HCl medium, *Corrosion Science*, **53**, 4265 (2011). Doi: <https://doi.org/10.1016/j.corsci.2011.08.038>
 54. T. A. Salman, A. A. Al-Amiery, L. M. Shaker, A. A. Kadhum, M. S. Takriff, A study on the inhibition of mild steel corrosion in hydrochloric acid environment by 4-methyl-2-(pyridin-3-yl) thiazole-5-carbohydrazide, *International Journal of Corrosion and Scale Inhibition*, **8**, 1035 (2019). Doi: <https://doi.org/10.17675/2305-6894-2019-8-4-14>
 55. H. J. Habeeb, H. M. Luaibi, T. A. Abdullah, R. M. Dakhil, A. A. Kadhum, A. A. Al-Amiery, Case study on thermal impact of novel corrosion inhibitor on mild steel, *Case Studies in Thermal Engineering*, **12**, 64 (2018). Doi: <https://doi.org/10.1016/j.csite.2018.03.005>
 56. M. A. Quraishi, H. K. Sharma, 4-Amino-3-butyl-5-mercapto-1, 2, 4-triazole: A new corrosion inhibitor for mild steel in sulphuric acid, *Materials Chemistry and Physics*, **78**, 18 (2003). Doi: [https://doi.org/10.1016/S0254-0584\(02\)00313-9](https://doi.org/10.1016/S0254-0584(02)00313-9)
 57. T. Poornima, J. Nayak, A. N. Shetty, Corrosion inhibition of the annealed 18 Ni 250 grade maraging steel in 0.67 m phosphoric acid by 3, 4-dimethoxybenzaldehydethiosemicarbazone, *Chemical Sciences Journal*, **69**, 1 (2012). <https://www.hilarispublisher.com/open-access/corrosion-inhibition-of-the-annealed-ni-grade-maraging-steel-in-m-phosphoric-acid-by-dimethoxybenzaldehydethiosemicarbazone.2150-3494.1000048.pdf>
 58. M. Abdallah, E. A. Helal, A. S. Fouda, Aminopyrimidine derivatives as inhibitors for corrosion of 1018 carbon steel in nitric acid solution, *Corrosion Sciences*, **48**, 1639 (2006). Doi: <https://doi.org/10.1016/j.corsci.2005.06.020>
 59. T. A. Salman, Q. A. Jawad, M. A. Hussain, A. A. Al-Amiery, L. Mohamed, A. A. Kadhum, M. S. Takriff, Novel ecofriendly corrosion inhibition of mild steel in strong acid environment: Adsorption studies and thermal effects, *International Journal of Corrosion and Scale Inhibition*, **8**, 1123 (2019). Doi: <https://doi.org/10.17675/2305-6894-2019-8-4-19>
 60. A. A. Alamiery, W. N. Wan Isahak, M. S. Takriff, Inhibition of Mild Steel Corrosion by 4-benzyl-1-(4-oxo-4-phenylbutanoyl) thiosemicarbazide: Gravimetric, Adsorption and Theoretical Studies, *Lubricants*, **9**, 93 (2021). Doi: <https://doi.org/10.3390/lubricants9090093>
 61. D. M. Jamil, A. K. Al-Okbi, M. M. Hanon, K. S. Rida, A. F. Alkaim, A. A. Al-Amiery, A. Kadhim, A. A. Kadhum, Carboethoxythiazole corrosion inhibitor: As an experimentally model and DFT theory, *Journal of Engineering and Applied Sciences*, **13**, 3952 (2018). Doi: <https://doi.org/10.36478/jeasci.2018.3952.3959>
 62. A. Y. Musa, W. Ahmoda, A. A. Al-Amiery, A. A. Kadhum, A. B. Mohamad, Quantum chemical calculation for the inhibitory effect of compounds, *Journal of Structural Chemistry*, **54**, 301 (2013). Doi: <https://doi.org/10.1134/S0022476613020042>
 63. S. Al-Baghdadi, T. S. Gaaz, A. Al-Adili, A. A. Al-Amiery, M. S. Takriff, Experimental studies on corrosion inhibition performance of acetylthiophene thiosemicarbazone for mild steel in HCl complemented with DFT investigation, *International Journal of Low-Carbon Technologies*, **16**, 181 (2021). Doi: <https://doi.org/10.1093/ijlct/ctaa050>
 64. A. Al-Amiery, T. A. Salman, K. F. Alazawi, L. M. Shaker, A. A. Kadhum, M. S. Takriff, Quantum chemical elucidation on corrosion inhibition efficiency of Schiff base: DFT investigations supported by weight loss and SEM techniques, *International Journal of Low-Carbon Technologies*, **15**, 202 (2020). Doi: <https://doi.org/10.1093/ijlct/ctz074>
 65. T. A. Salman, K. F. Al-Azawi, I. M. Mohammed, S. B. Al-Baghdadi, A. A. Al-Amiery, T. S. Gaaz, A. A. Kadhum, Experimental studies on inhibition of mild steel corrosion by novel synthesized inhibitor complemented with quantum chemical calculations, *Results in Physics*, **10**, 291 (2018). Doi: <https://doi.org/10.1016/j.rinp.2018.06.019>
 66. D. S. Zinad, M. Hanoon, R. D. Salim, S. I. Ibrahim, A. A. Al-Amiery, M. S. Takriff, A. A. Kadhum, A new synthesized coumarin-derived Schiff base as a corrosion inhibitor of mild steel surface in HCl medium: Gravimetric and DFT studies, *International Journal of Corrosion and*

- Scale Inhibition*, **9**, 228 (2020). Doi: <https://doi.org/10.17675/2305-6894-2020-9-1-14>
67. A. A. Alamiery, Effect of Temperature on the Corrosion Inhibition of 4-ethyl-1-(4-oxo-4-phenylbutanoyl), *Letters in Applied NanoBioScience*, **11**, 3502 (2022). Doi: <https://doi.org/10.33263/LIANBS112.35023508>
68. D. S. Zinad, Q. A. Jawad, M. A. Hussain, A. Mahal, L. Mohamed, A. A. Al-Amiery, Adsorption, temperature and corrosion inhibition studies of a coumarin derivatives corrosion inhibitor for mild steel in acidic medium: Gravimetric and theoretical investigations, *International Journal of Corrosion and Scale Inhibition*, **9**, 134 (2020). Doi: <https://doi.org/10.17675/2305-6894-2020-9-1-8>
69. J. A. Yamin, E. A. Sheet, A. Al-Amiery, Statistical analysis and optimization of the corrosion inhibition efficiency of a locally made corrosion inhibitor under different operating variables using RSM, *International Journal of Corrosion and Scale Inhibition*, **9**, 502 (2020). Doi: <https://doi.org/10.17675/2305-6894-2020-9-2-6>
70. T. A. Salman, D. S. Zinad, S. H. Jaber, M. Al-Ghezi, A. Mahal, M. S. Takriff, A. A. Al-Amiery, Effect of 1, 3, 4-thiadiazole scaffold on the corrosion inhibition of mild steel in acidic medium: An experimental and computational study, *Journal of Bio-and Tribo-Corrosion*, **5**, 11 (2019). Doi: <https://doi.org/10.1007/s40735-019-0243-7>
71. S. B. Al-Baghdadi, A. A. Al-Amiery, A. A. Kadhum, M. S. Takriff, Computational Calculations, Gravimetric, and Surface Morphological Investigations of Corrosion Inhibition Effect of Triazole Derivative on Mild Steel in HCl, *Journal of Computational and Theoretical Nanoscience*, **17**, 2897 (2020). Doi: <https://doi.org/10.1166/jctn.2020.9328>
72. M. M. Hanoon, Z. A. Gbashi, A. A. Al-Amiery, A. Kadhim, A. A. Kadhum, M. S. Takriff, Study of Corrosion Behavior of N'-acetyl-4-pyrrol-1-ylbenzohydrazide for Low-Carbon Steel in the Acid Environment: Experimental, Adsorption Mechanism, Surface Investigation, and DFT Studies, *Progress in Color Colorants and Coatings*, **15**, 133 (2022). https://pccc.icrc.ac.ir/article_81789_a8a7e55e3fc95bcf7aa223671e4f8495.pdf
73. M. M. Hanoon, A. M. Resen, A. A. Al-Amiery, A. A. Kadhum, M. S. Takriff, Theoretical and Experimental Studies on the Corrosion Inhibition Potentials of 2-((6-Methyl-2-Ketoquinolin-3-yl) Methylene) Hydrazinecarbothioamide for Mild Steel in 1 M HCl, *Progress in Color Colorants and Coatings*, **15**, 11 (2022). Doi: <https://doi.org/10.30509/PCCC.2020.166739.1095>